

Activation Energy of Alumina Dissolution in FeO-Bearing Slags

Taejun Kwack¹, Hyungsic Um² and Yongsug Chung^{1,*}

¹ Department of Advanced Materials Engineering, Technical University of Korea, 237, Sangidaehak-ro, Shiheung-si 15073, Republic of Korea

² R&D Center, Dongkuk Steel Company, 70, Geonposaneop-ro 3214beon-gil, Nam-gu, Pohang-si 37874, Republic of Korea

* Correspondence: ychung@tukorea.ac.kr

Abstract: The dissolution of Al₂O₃ non-metallic inclusions in slag containing FeO was investigated in this study. The slag system used in the experiments was a quaternary system of CaO-SiO₂-Al₂O₃-FeO. The composition of the slag was studied by fixing the basicity (CaO/SiO₂ ratio) to 1 and varying the FeO content to 10 and 20 wt%. In addition, the experimental temperature was varied to 1550 °C, 1575 °C, and 1600 °C to study the effect of temperature on the Al₂O₃ dissolution behavior. The experimental equipment used was a single hot thermocouple apparatus. The dissolution rate of Al₂O₃ particles increased linearly with increasing temperature and FeO content. In addition, the mass transfer activation energy of Al₂O₃ dissolution in FeO 10 wt% and FeO 20 wt% was calculated through an Arrhenius-type analysis. The obtained mass transfer activation energies were 159 and 189 kJ/mole, respectively.

Keywords: non-metallic inclusions; Al₂O₃ dissolution; activation energy; refining

1. Introduction

In line with South Korea's 2030 carbon neutrality goal, the steel industry is increasingly interested in electric arc furnaces, which emit less carbon dioxide than blast furnaces. Accordingly, research on electric arc furnace processes is necessary [1]. The electric arc furnace process injects oxygen into the steel to reduce operating time, oxidation refining, etc. [2]. The presence of oxygen in the steel can cause problems such as corrosion and hot shortness. Therefore, a deoxidation process is essential [3]. The deoxidation process is mainly carried out using aluminum, which is a strong deoxidizer [4]. When tapping molten steel, aluminum is added to the ladle furnace to deoxidize it [5]. This process produces Al₂O₃ inclusions, which cause several problems including fatigue failure of the steel and nozzle clogging [6]. It is therefore important to remove Al₂O₃ inclusions as slag.

There are two ways to remove Al₂O₃ inclusions. The first is Ca treatment, where the Al₂O₃ inclusions are removed by adding Ca to transform the Al₂O₃-inclusion solid phase to a liquid CaO-Al₂O₃ phase [7]. However, this method has the disadvantage of interaction with the bottom lining refractory, which causes corrosion of the refractory. In addition, CaS inclusions, which are as harmful as Al₂O₃ inclusions, are easily formed [6]. The second is to float and separate Al₂O₃ inclusions to the slag/metal interface in a ladle refining process and then dissolve and remove them from the top layer of slag [8]. This method has been used not only in electric furnace processes, but also in blast furnace processes. For this reason, the dissolution behavior of non-metallic inclusions in slag has been extensively studied during the past 30 years.

Sridhar et al. [9] studied the dissolution behavior of Al₂O₃ particles in CaO-SiO₂-Al₂O₃-MgO slag with temperature as a variable. They reported that the dissolution of Al₂O₃ is dominated by mass transfer through the boundary layer. Q. Shu et al. [10] investigated the effect of Na₂O addition on the dissolution behavior of cylindrical Al₂O₃ in CaO-Al₂O₃-MgO-SiO₂ slag. They reported that the dissolution mechanism of Al₂O₃



Citation: Kwack, T.; Um, H.; Chung, Y. Activation Energy of Alumina Dissolution in FeO-Bearing Slags. *Metals* **2023**, *13*, 1702. <https://doi.org/10.3390/met13101702>

Academic Editor: Zhiyin Deng

Received: 31 August 2023

Revised: 26 September 2023

Accepted: 27 September 2023

Published: 6 October 2023



Copyright: © 2023 by the authors. Licensee MDPI, Basel, Switzerland. This article is an open access article distributed under the terms and conditions of the Creative Commons Attribution (CC BY) license (<https://creativecommons.org/licenses/by/4.0/>).

is boundary layer mass transfer, and the dissolution rate of cylindrical Al_2O_3 increases with a decrease in slag viscosity and increase in thermodynamic driving force with Na_2O addition. Yi. K. Wi et al. [11] investigated the dissolution behavior of Al_2O_3 and MgO particles within Al_2O_3 - CaO - MgO slag, with temperature as the variable. Their research revealed that the dissolution kinetics of Al_2O_3 particles are primarily influenced by diffusion processes, whereas the dissolution of MgO particles adheres to chemical reaction kinetics. C. Ren et al. [12] examined how Al_2O_3 particles dissolve within CaO - Al_2O_3 - SiO_2 slag, considering variations in slag composition and temperature. They reported that the rate-limiting step of Al_2O_3 particle dissolution in CaO - Al_2O_3 - SiO_2 slag is diffusion in liquid slag, and an increase in C/A ($\text{CaO}/\text{Al}_2\text{O}_3$ ratio) and C/S (CaO/SiO_2 ratio) increased the dissolution rate of Al_2O_3 particles. L. Holappa et al. [13] studied the dissolution behavior of Al_2O_3 particles and $\text{MgO}\cdot\text{Al}_2\text{O}_3$ particles in CaO - SiO_2 - Al_2O_3 - MgO slag with basicity as a variable. They reported that Al_2O_3 particles and $\text{MgO}\cdot\text{Al}_2\text{O}_3$ particles dissolve slowly in slag with low basicity, and the dissolution rate of the particles increases in slag with low viscosity. H. Um et al. [5] investigated the dissolution behavior of Al_2O_3 particles in CaO - SiO_2 - Al_2O_3 - Fe_xO slag with Fe_xO content as a variable. They reported that as the Fe_xO content increased from 0 to 20 wt%, the dissolution rate of Al_2O_3 particles increased due to the decrease in viscosity. However, when the Fe_xO content increased to 30 wt%, the dissolution rate did not increase due to the formation of the CA6 phase at the Al_2O_3 particle interface. Y. Park et al. [14] studied the dissolution behavior of wall-type Al_2O_3 in CaO - Al_2O_3 - Fe_xO - MgO - SiO_2 slag with C/A and Fe_xO content as variables. They reported that increasing temperature, increasing C/A , and increasing Fe_xO content increased the dissolution rate of Al_2O_3 . They also conducted temperature-variable experiments on slag with one composition to derive the mass transport activation energy of Al_2O_3 dissolution, which they reported to be 193.6 kJ/mole. S. Yeo et al. [15] conducted a study on the dissolution behavior of Al_2O_3 particles in CaO - Al_2O_3 - SiO_2 slag with Al_2O_3 composition and the temperature of the slag as variables. The investigators found that the dissolution rate increased with the increasing activity of Al_2O_3 . In addition, they reported that the diffusion activation energy of Al_2O_3 dissolution was in a range of about 320 to 490 kJ/mole, depending on the composition of Al_2O_3 in the slag.

In addition, the dissolution behavior of Al_2O_3 in slags under various conditions has been studied [16–20]. However, since electric arc furnace slags use Fe scrap as raw material, the content of FeO in the slag increases [2]. For this reason, the composition of the slag used in electric furnace research must include FeO . However, there has been little research on the dissolution behavior of non-metallic inclusions in slag containing FeO . In addition, the temperature of electric arc furnace slag varies from 1550 to 1700 °C, but few studies have been conducted with temperature as a variable in slag containing FeO [21]. For this reason, the dissolution behavior of Al_2O_3 particles in CaO - SiO_2 - Al_2O_3 - FeO slag was studied in this work with temperature and FeO content as variables.

2. Materials and Methods

2.1. Sample Preparation

Table 1 shows the chemical composition and diameter of the Al_2O_3 particles used in the experiment. The shape of Al_2O_3 particles is spherical, with a diameter of $500 \pm 2.5 \mu\text{m}$ (Goodfellow Cambridge limited, Cambridgeshire, UK). The average weight of the particles was 0.25 mg, and the purity of the Al_2O_3 was 99.9%.

Table 1. Chemical compositions and diameter of Al_2O_3 particles.

Type	Source	Diameter	Weight	Concentration	
				Al_2O_3 (%)	Other (%)
Alumina sphere	GoodFellow	$500 \pm 2.5 \mu\text{m}$	$0.25 \pm 0.05 \text{ mg}$	99.9	0.1

Table 2 shows the chemical composition and basicity of the slag used in the experiments. The basicity was fixed at 1, and the FeO content was varied from 10 to 20 wt%. The amount of slag used in each experiment was set to 4 mg for stability in the experiment. The slag was prepared by mixing CaO powder, prepared by calcining CaCO₃ at 1200 °C with Al₂O₃ and FeO powder individually, and melting them in a high-frequency induction furnace.

Table 2. Chemical compositions of slag (wt%).

Headings	CaO	SiO ₂	Al ₂ O ₃	FeO	Basicity	References
Slag0	47.5	47.5	5	0	1	[15]
Slag1	43.7	42.6	4.6	9.1	1	
Slag2	37.7	38.4	4.4	19.5	1	
Slag3	32.5	32.5	5	30	1	[5]

2.2. Single Hot Thermocouple Apparatus (SHT Apparatus)

In this study, we observed the dissolution behavior of Al₂O₃ particles using a single hot thermocouple (SHT) apparatus. Figure 1 is a schematic diagram of the SHT apparatus. It consisted of a B-type thermocouple to melt slag and dissolve Al₂O₃ particles, an SHT controller to control and check the temperature of the B-type thermocouple, a video camera to observe and record the dissolution behavior of Al₂O₃ particles in real time, and an optical microscope.

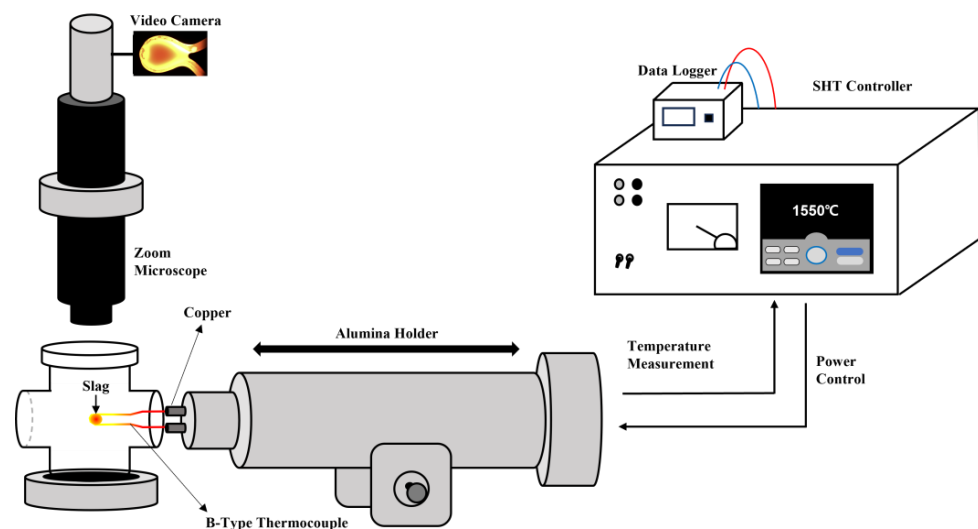


Figure 1. Schematic diagram of single hot thermocouple apparatus.

The SHT apparatus has several advantages, including the ability to inject Al₂O₃ particles at the desired temperature range, quenching at 300 °C/s using the SHT controller, ease of preparing quenching specimens, and real-time observation of the melting behavior of Al₂O₃ particles with a video camera and optical microscope.

2.3. Experimental Conditions

Figure 2 shows the process of the Al₂O₃ particle dissolution experiment using the SHT apparatus. First, the + and – poles of the B-type thermocouple were welded to form an oval shape, and then mounted on the copper tip. The slag was then placed on the B-type thermocouple and the temperature was raised to 8 °C/s using an SHT controller to melt the slag. When the experimental temperature (1550, 1575, 1600 °C) was reached, Al₂O₃ particles were added to the melted slag to dissolve it. Subsequently, after the set time (120, 240, 360 sec), quenching was performed using the SHT controller.

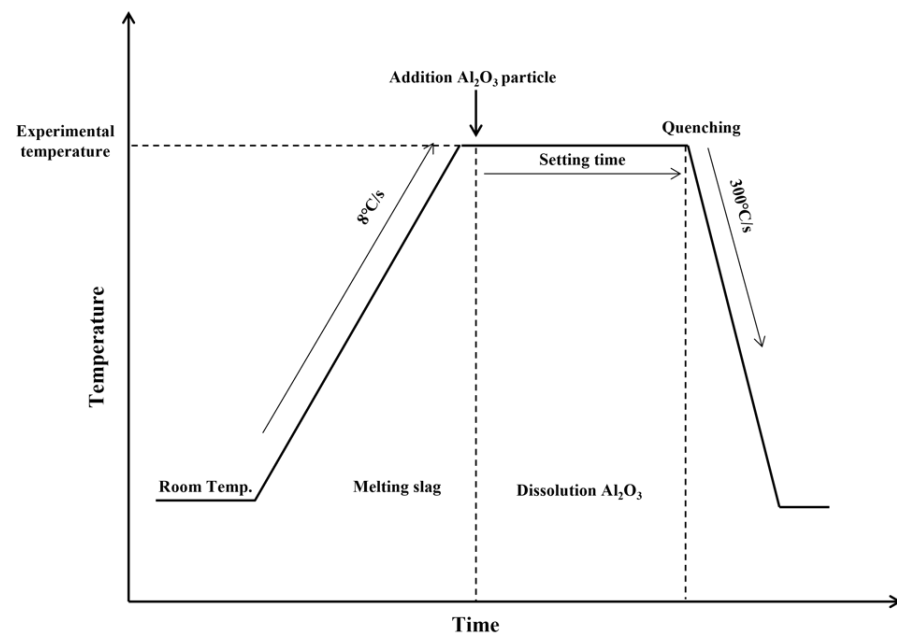


Figure 2. Experimental procedure of Al₂O₃ particle dissolution.

As mentioned earlier, the SHT apparatus has the advantage of allowing observation of the dissolution behavior of Al₂O₃ particles in real time. Several studies using this apparatus have taken advantage of this by observing the dissolution behavior of inclusions in real time [5,15,22,23]. However, in this study, there was a problem, as the dissolution behavior of Al₂O₃ particles could not be observed in real time due to the opacity of the slag at high temperature because it contained FeO, a transition metal. To solve this problem, quenching specimens were prepared by exploiting one of the advantages of the SHT apparatus, i.e., that quenching at 300 °C/s is possible. The quenching specimens were then polished, and the diameter was measured in four directions, as shown in Figure 3a, to check the dissolution rate of the Al₂O₃ particles. However, using this method, only a small portion of the diameter of the Al₂O₃ particles may be exposed. For this reason, the largest diameter value found by repeating the polishing several times was set as the representative value of the Al₂O₃ particle dissolution rate, as shown in Figure 3b.

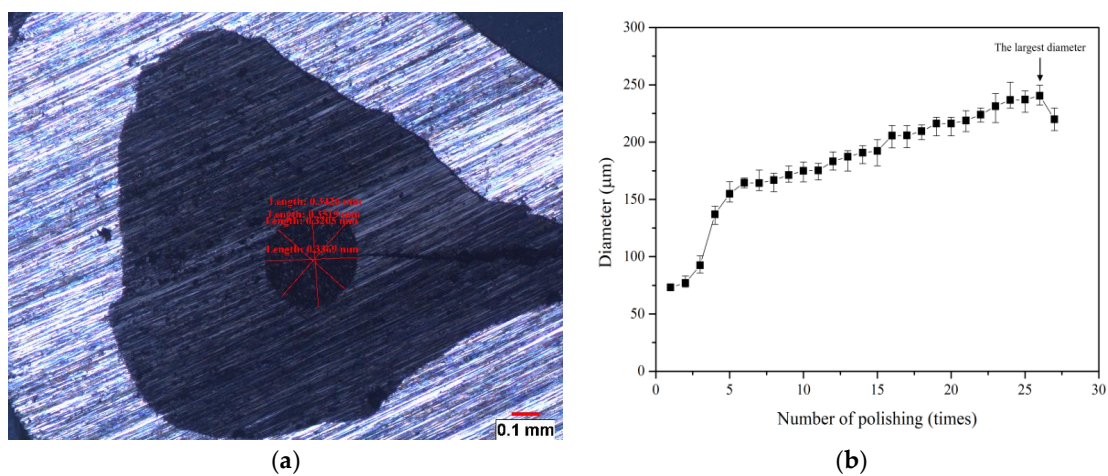


Figure 3. Measurement of alumina diameter in opaque slag: (a) measurement of Al₂O₃ particle in polished quenching specimens; (b) the largest diameter of Al₂O₃ particles found through multiple polishings.

The quenching specimens were also analyzed using SEM to identify the reaction layer at the interface between the slag and Al_2O_3 particles. No compounds were observed at the interface in the specimens.

3. Results and Discussion

3.1. Dissolution Behavior of Al_2O_3 Particles according to Temperature and FeO Content in Slag

The SHT apparatus was used to assess the dissolution behavior of Al_2O_3 particles in slag with changing FeO content. The experiment temperatures were 1550, 1575, and 1600 °C, and the experiment times were 120, 240, and 360 s for each condition. Experiments were performed at least three times for each condition for reproducibility.

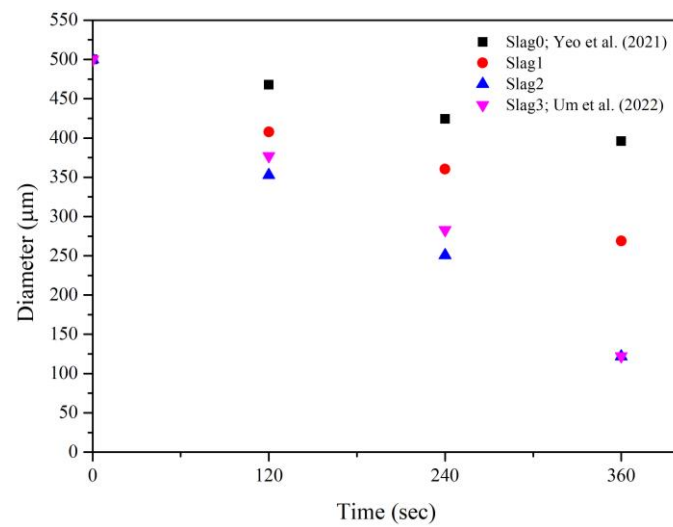
The variation in the diameter of Al_2O_3 particles in slags with different FeO contents at each temperature is shown in Figure 4. Slag0 and slag3 are based on previous papers [5,15]. In the case of slag3, it was not possible to conduct experiments at temperatures above 1550 °C due to the short circuit of B-type thermocouples at high temperatures. Also, in the case of slag0, the temperature deviation was increased by 50 °C, and hence there are no data at 1575 °C.

Figure 4a shows the dissolution behavior of Al_2O_3 particles at 1550 °C. The diameter of the Al_2O_3 particles decreased linearly with the dissolution time, and the dissolution rate increased as the FeO content in the slag increased. However, for slag3, the dissolution rate did not increase with the increasing FeO content. These experimental results were ascribed to the generation of the CA6 phase at the interface of Al_2O_3 particles and slag under the experimental conditions of slag3, which changed the dissolution process of the particles into an inter-compound chemical reaction [5]. Figure 4b shows the dissolution behavior of Al_2O_3 particles at 1575 °C. The results of the experiment at 1575 °C showed that the diameter of the Al_2O_3 particles decreased linearly with the dissolution time, and the dissolution rate increased with an increase in FeO content in the slag. Figure 4c shows the dissolution behavior of the Al_2O_3 particles at 1600 °C. The results of the experiment at 1600 °C showed that the diameter of the Al_2O_3 particles decreased linearly with the dissolution time, and the dissolution rate increased with an increase in FeO content in the slag. However, at 1600 °C in the slag2 experiment, the Al_2O_3 particles completely dissolved before 360 s. For this reason, additional experiments were conducted at 300 s for an accurate interpretation.

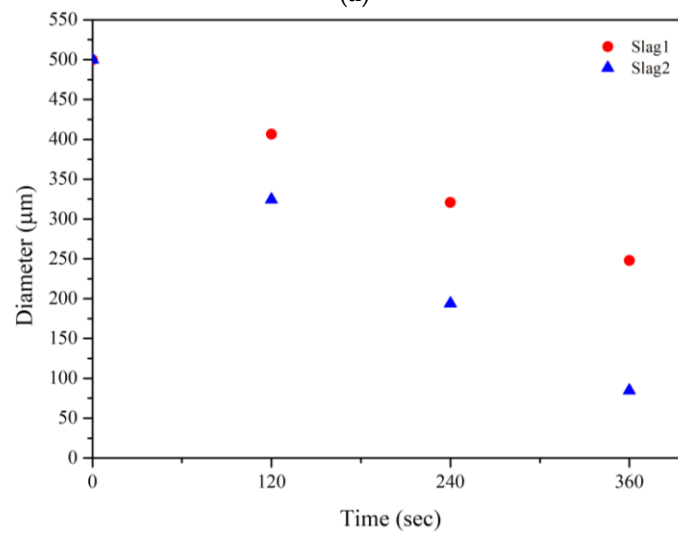
Table 3 lists the particle diameters of the Al_2O_3 particles for each condition.

Table 3. Diameter of Al_2O_3 particles according to FeO content and temperature (μm).

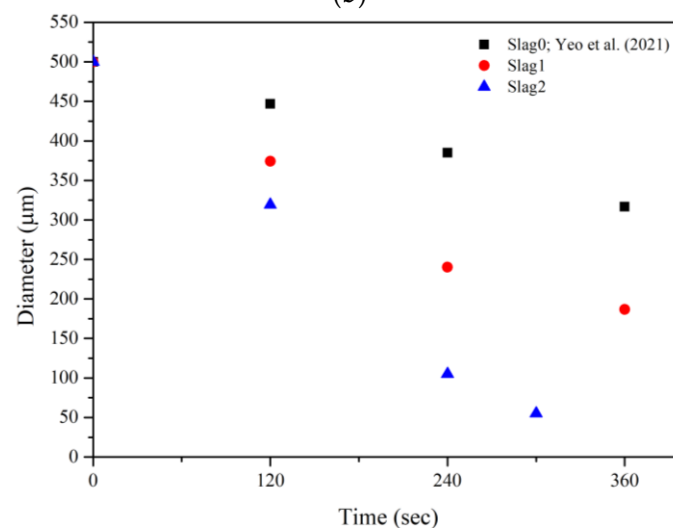
Temperature (°C)	Slag	120 s	240 s	360 s	References
1550	0	465	420	393	[15]
	1	408	360	269	
	2	353	251	122	
	3	377	283	122	[5]
1575	1	407	321	248	
	2	324	194	85	
1600	0	447	385	317	[15]
	1	374	240	187	
	2	319	105	55 (300 s)	



(a)



(b)



(c)

Figure 4. Al_2O_3 particle dissolution behavior according to FeO content and temperature: (a) 1550 °C; (b) 1575 °C; (c) 1600 °C. Data by Yeo et al. refer to Ref. [15]; Data by Um et al. refer to Ref. [5].

3.2. Analysis of Slag/ Al_2O_3 Particle Interface through SEM

As previously described, H. Um et al. [5] reported that for slag3, a CA6 phase was created at the interface of slag and Al_2O_3 particles, which changed the dissolution process of the Al_2O_3 particles. In addition, Park et al. [8] reported that a ring-shaped compound was formed along the particle/slag interface depending on the slag composition. For this reason, to better understand the dissolution behavior of Al_2O_3 particles in the experimental slag, the interface of slag and Al_2O_3 particles was analyzed using SEM and EDS. Figure 5 shows the results of SEM and EDS analysis for the interface of slag1, slag2, and Al_2O_3 particles under the condition of 1550 °C.

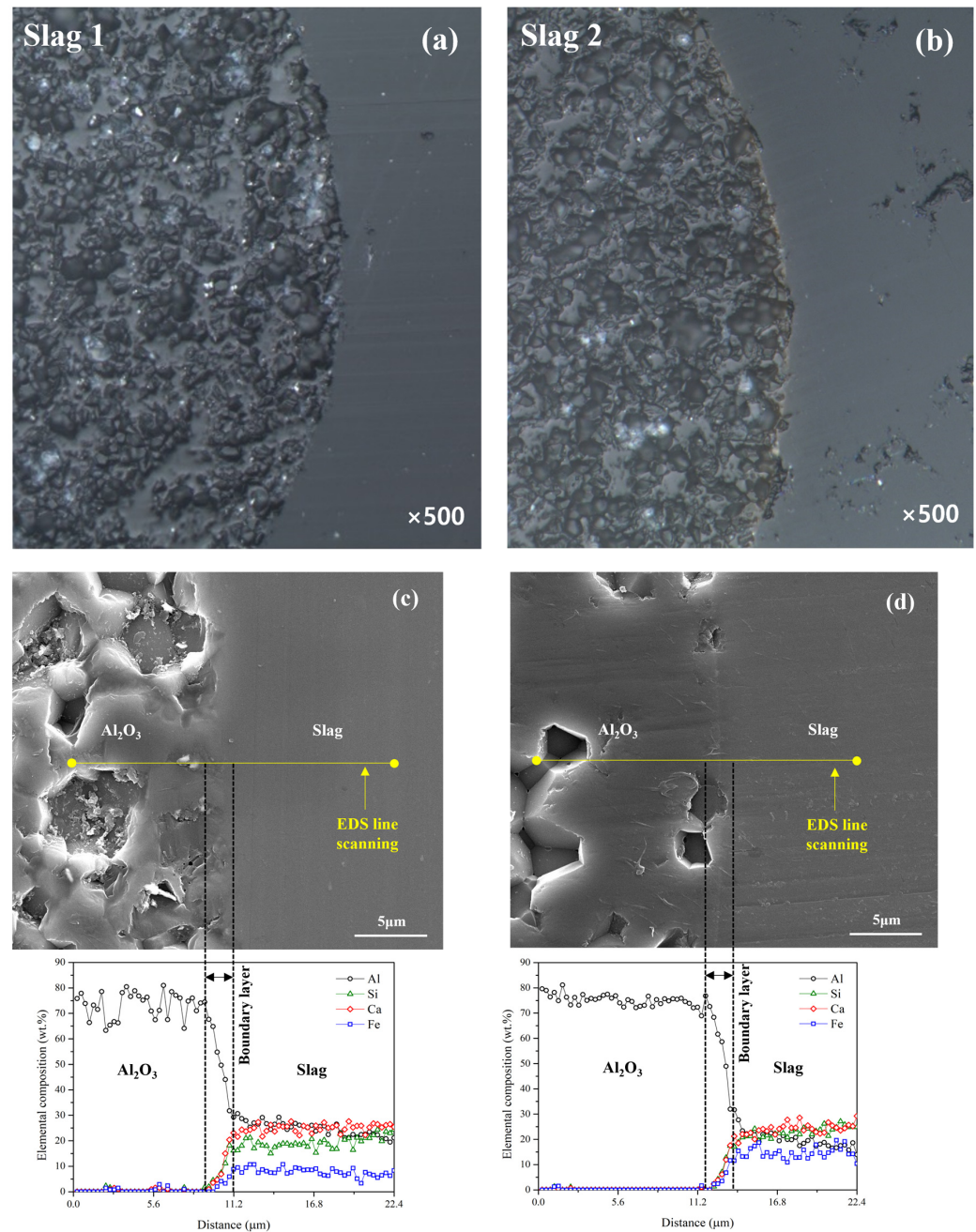


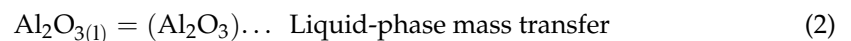
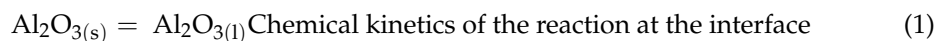
Figure 5. Cross-sectional image of Al_2O_3 particles from SEM: (a) Al_2O_3 particle in slag1; (b) Al_2O_3 particle in slag2; and spectrum of EDS line scanning of Al, Si, Ca, and Fe at the Al_2O_3 particles/slag interface; (c) Al_2O_3 particle/slag1; (d) Al_2O_3 particle/slag2.

From Figure 5a,b, it can be seen that no compounds were formed at the interface of slag1, slag2, and Al₂O₃ particles. It was also confirmed that no compounds were formed at the interface at 1550, 1575, or 1600 °C. S. Yeo et al. [15] and Taira et al. [24] reported that the dissolution rate of Al₂O₃ in CaO-SiO₂-Al₂O₃ slag was controlled by diffusion in the boundary layer. Also, H. Um et al. [5] reported that the dissolution of Al₂O₃ particles in CaO-SiO₂-Al₂O₃-Fe_xO slag was controlled by diffusion in the boundary layer of slag and Al₂O₃ particles if no compounds were generated at the interface of slag and Al₂O₃ particles. Furthermore, in the present study, it can be seen from Figure 5c,d that the concentration of Al decreased linearly along the boundary layer from Al₂O₃ particles to slag. On the other hand, the concentrations of Ca, Si, and Fe were found to have increased linearly. For this reason, it was determined that Al₂O₃ in the boundary layer exhibited diffusion behavior.

Therefore, no compounds were formed at the interface of Al₂O₃ particles and slag under the conditions of this study, and based on the EDS results of the interface, it is believed that for the dissolution mechanism of Al₂O₃ particles in slag1 and slag2 it was only necessary to consider the behavior by diffusion in the boundary layer.

3.3. Dissolution Mechanism of Al₂O₃

Solid Al₂O₃ particles can be dissolved by liquid slag through the following process [5].



In other words, the dissolution of solid Al₂O₃ particles in liquid slag can be controlled by a chemical reaction or liquid-phase mass transfer [8,24–26]. It is understood that the dissolution of Al₂O₃ particles in liquid slag is controlled by liquid-phase mass transfer in the boundary layer unless a compound is generated at the interface of Al₂O₃ particles and slag [9,19,25,27–30]. As noted above, no compounds were generated at the interface of Al₂O₃ particles and slag under the present experimental conditions. Therefore, the rate-controlling step of Al₂O₃ particle dissolution in this experiment can be interpreted as liquid-phase mass transfer at the boundary layer.

If the rate-controlling step in the dissolution of Al₂O₃ in slag is liquid-phase mass transfer in the boundary layer, then the relationship between the mass transfer flux and mass transfer coefficient of Al₂O₃ particle dissolution can be expressed by the mass transfer equation as follows [31]:

$$J = -k(C_i - C_b) \quad (3)$$

where J is the mass transfer flux; k is the mass transfer coefficient in the slag; C_i and C_b are the Al₂O₃ content at the interface and in bulk slag; and $(C_i - C_b)$ is the driving force of the dissolution.

If the Al₂O₃ particles being dissolved are spherical, then Equation (3) can be transformed into the following dissolution rate equation [31]:

$$\frac{dr}{dt} = -k(C_i - C_b)M/\rho \quad (4)$$

where r is the radius of the Al₂O₃ particles; dr/dt is the dissolution rate; M is the molecular weight of Al₂O₃; and ρ is the slag density.

The dissolution rate can be calculated from the experimental data, as shown in Figure 6, and the slag density and driving force of the dissolution can be obtained using FactSage^{7.3}TM; hence, the mass transfer coefficient according to temperature and FeO content can be derived using Equation (4). The physical properties and mass transfer coefficients for each temperature and FeO content are summarized in Table 4.

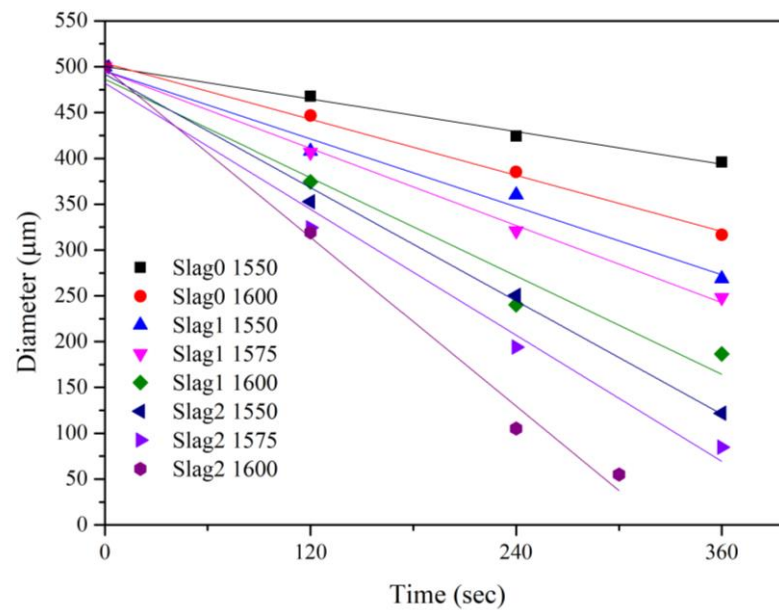


Figure 6. Dissolution rate by temperature and FeO content.

Table 4. Physical properties and mass transfer coefficient according to temperature and FeO content.

	Driving Force of Dissolution ΔC (mole/m ³) *FactSage ^{7.3} TM	Slag Density (ρ) (kg/m ³)	Dissolution Rate $\left(\frac{dr}{dt}\right)$ (cm/s)	Mass Transfer Coefficient (k) (cm/s)	References
Slag0 1550 °C	10,745	2660	2.96×10^{-5}	7.19×10^{-8}	[15]
Slag0 1600 °C	11,399	2647	5.10×10^{-5}	1.16×10^{-7}	
Slag1 1550 °C	10,885	2796	6.18×10^{-5}	1.56×10^{-7}	Present study
Slag1 1575 °C	11,581	2789	7.01×10^{-5}	1.66×10^{-7}	
Slag1 1600 °C	11,846	2782	8.95×10^{-5}	2.06×10^{-7}	
Slag2 1550 °C	11,050	2943	1.03×10^{-4}	2.69×10^{-7}	Present study
Slag2 1575 °C	11,600	2935	1.15×10^{-4}	2.84×10^{-7}	
Slag2 1600 °C	11,925	2928	1.54×10^{-4}	3.71×10^{-7}	

The mass transfer coefficient increases with the FeO content in the slag and with increasing melting temperature.

3.4. Activation Energy

The activation energy of mass transfer—the dissolution mechanism of Al_2O_3 —can be quantitatively measured. In this study, the dissolution rate of Al_2O_3 particles was measured with temperature as a variable, and the mass transfer coefficient was calculated accordingly. By graphing the reciprocal of the mass transfer coefficient and temperature using the Arrhenius equation, which is expressed as follows, the activation energy for mass transfer can be derived [32]:

$$k = k_0 \cdot \exp\left(-\frac{E_k}{RT}\right) \quad (5)$$

where k is the mass transfer coefficient; k_0 is the pre-exponential constant; R is the universal gas constant; T is the absolute temperature; and E_k is the activation energy of mass transfer.

To explain how E_k is derived, substituting logarithms into the above expression, we can express it as a function of $\ln(k)$ and temperature, as follows:

$$\ln(k) = -\frac{E_k}{R} \frac{1}{T} + \ln k_0 \quad (6)$$

This expression tells us that the slope of the $\ln(k)-1/T$ graph is $-\frac{E_k}{R}$. Therefore, multiplying this value by $-R$ gives the activation energy for mass transfer. Cho et al. calculated the mass transfer coefficient by measuring the dissolution behavior of Al_2O_3 in $\text{CaO-SiO}_2\text{-Al}_2\text{O}_3$ slag with temperature as a variable, and derived the E_k of Al_2O_3 dissolution using the above method [31]. In this study, E_k was also calculated through the above process and is shown in Figure 7.

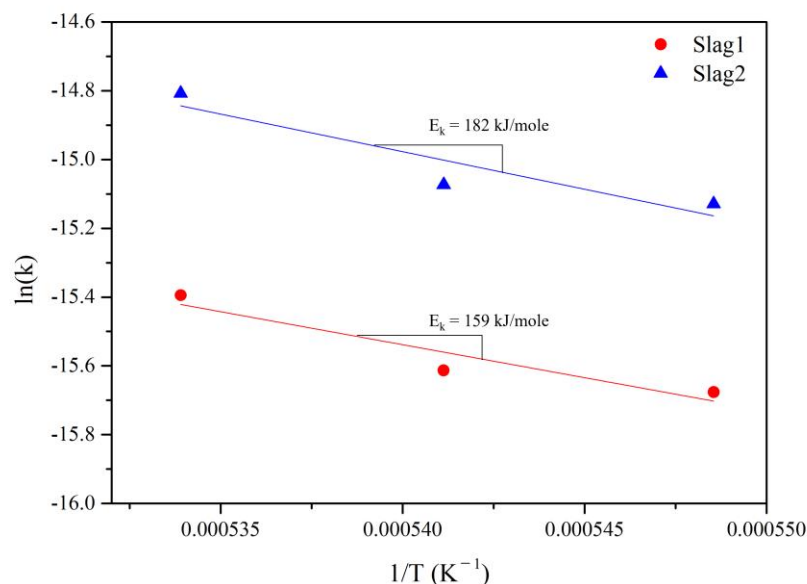


Figure 7. Arrhenius plot of the mass transfer coefficient.

The E_k of slag1 was calculated to be 159 kJ/mole and the E_k of slag2 was calculated to be 182 kJ/mole. In addition, the E_k of slag with FeO calculated in this study and the E_k values of slag without FeO calculated in other studies are summarized in Table 5.

Table 5. Comparison of Al_2O_3 dissolution E_k according to slag composition.

Slag	Chemical Composition (wt%)						E_k (kJ/mole)	References
	CaO	SiO ₂	Al ₂ O ₃	MgO	Ce ₂ O ₃	FeO		
0	47.5	47.5	5.0	0	0	0	304	[15]
1	42.5	42.5	5.0	0	0	10	159	Present study
2	37.5	37.5	5.0	0	0	20	182	
4	45.0	10.0	45.0	0	0	0	445	[31]
5	35.0	30.0	35.0	0	0	0	334	
6	45.0	4.5	37.5	10.0	3	0	292	[33] ¹
7	45.0	4.5	35.5	10.0	5	0	347	
8	45.0	4.5	32.5	10.0	8	0	249	

¹ Cylindrical Al_2O_3 rotated at 200 rpm.

From Table 5, the E_k of the experimental slag with FeO is lower than that of the slag without FeO, indicating that the Al_2O_3 dissolution in the slag with FeO is faster compared to that in the slag without FeO. In other words, when FeO is included in the slag, the mass transfer of Al_2O_3 particles is relatively easier and the dissolution of Al_2O_3 particles can be faster. This means that, as mentioned at the introduction, when slag is used to remove Al_2O_3 inclusions, electric furnace slag containing a large amount of FeO will be better at removing Al_2O_3 inclusions than blast furnace slag containing a trace amount of FeO.

3.5. Increased Dissolution Rate of Al_2O_3 by Increasing FeO Content

We can interpret the increase in the dissolution rate of Al_2O_3 particles with increasing FeO content in the slag in terms of viscosity and the driving force of dissolution. The viscosity of slag0, 1, and 2 at the experimental temperature was obtained using FactSage^{7.3TM}. Additionally, a phase diagram was drawn using FactSage^{7.3TM} and is shown in Figure 8, and the driving force for dissolution of Al_2O_3 particles was obtained using this. We used FactPS, FT oxid, and FS stel databases of FactSage^{7.3TM} to draw the state diagram. The results are summarized in Table 6.

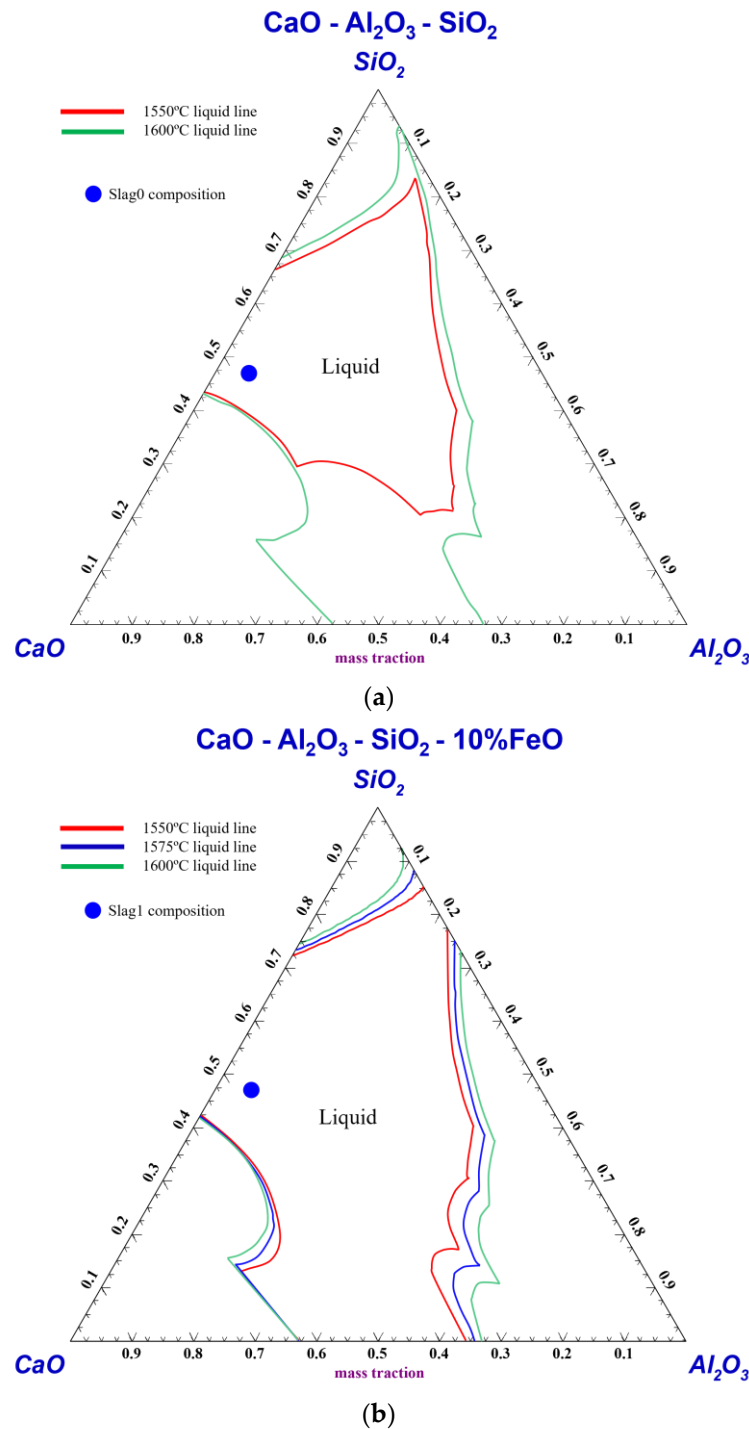


Figure 8. Cont.

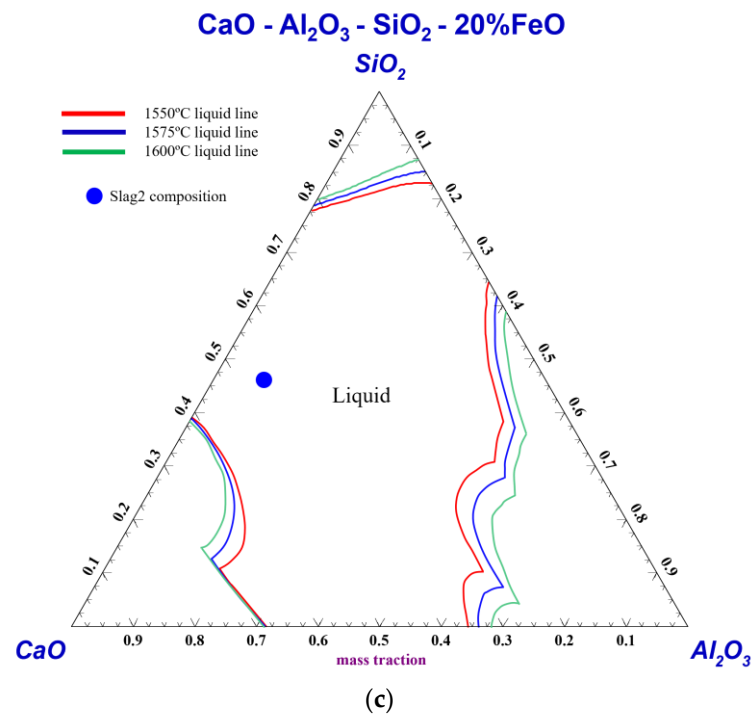


Figure 8. CaO-Al₂O₃-SiO₂-FeO phase diagram and composition of each slag at the experiment temperature: (a) slag0; (b) slag1; and (c) slag2.

Table 6. Slag viscosity and Al₂O₃ particle driving force of dissolution by temperature and FeO content.

Headings	Slag Viscosity (Pa·s) *FactSage ^{7.3TM}	Driving Force of Dissolution (ΔC) (mole/m ³) *FactSage ^{7.3TM}	References
Slag0 1550 °C	3.235	10,745	[15]
Slag0 1600 °C	2.202	11,399	
Slag1 1550 °C	0.159	10,885	Present study
Slag1 1575 °C	0.140	11,581	
Slag1 1600 °C	0.124	11,846	
Slag2 1550 °C	0.098	11,050	Present study
Slag2 1575 °C	0.087	11,600	
Slag2 1600 °C	0.078	11,925	

From Figure 8, it can be seen that the liquid-phase area increased with increasing FeO content and temperature, which also increased the driving force of dissolution.

From Table 6, it can be seen that the viscosity of the slag decreased and Al₂O₃ driving force of dissolution increased as the FeO content increased.

In summary, as the FeO content in the slag increased, the slag viscosity decreased and the driving force of Al₂O₃ dissolution increased. In addition, in this study, the mechanism of Al₂O₃ dissolution was mass transfer. Therefore, the slag viscosity, the driving force of dissolution of Al₂O₃ particle, and the dissolution rate of Al₂O₃ particle have the following relationship [34,35]:

$$\log(r) \propto \log\left(\frac{\Delta C}{\eta}\right) \quad (7)$$

where r is the dissolution rate of Al₂O₃; ΔC is the driving force for the dissolution of Al₂O₃; and η is the slag viscosity.

To summarize this equation and the above relationship, as the FeO content increased, the viscosity decreased, and the driving force of Al_2O_3 particle dissolution increased, increasing the dissolution rate of Al_2O_3 dissolution. In fact, the result of this experiment shows that the dissolution rate increased as the FeO content increased. In other words, it can be seen that the results of the experiment fit well with the relationship of Equation (7). In addition, FeO was added and the viscosity decreased, so diffusion occurred more easily. As a result, the liquid-phase mass transfer was accelerated, and the mass transfer coefficient increased.

4. Conclusions

In this study, the dissolution behavior of Al_2O_3 was studied by varying the FeO content in the slag from 10 to 20 wt%, and temperatures of 1550 °C, 1575 °C, and 1600 °C. The results were as follows:

- (1) The dissolution rate increased linearly as the FeO content of the slag increased from 0 to 20 wt% and the dissolution temperature increased from 1550 to 1600 °C.
- (2) Through an SEM and EDS analysis, it was observed that no compound was formed at the interface of Al_2O_3 particles and slag. In addition, it was observed that the concentration of Al in the boundary layer decreased linearly as it moved from Al_2O_3 particles to slag. Therefore, the rate step of Al_2O_3 particle dissolution is interpreted as liquid-phase mass transfer.
- (3) The mass transfer coefficient was obtained using the dissolution rate equation. The mass transfer coefficient increased with increasing FeO content in the slag and increasing dissolution temperature.
- (4) The mass transfer coefficient was plotted in a graph as a function of temperature, and the E_k values of slag1 and slag2 (159 and 182 kJ/mole, respectively) were found using the Arrhenius equation.
- (5) The E_k of Al_2O_3 mass transfer in slag containing FeO in this study was lower than the E_k of slag without FeO.
- (6) As the FeO content in the slag increased, the viscosity decreased and Al_2O_3 dissolution driving force increased, resulting in an increase in the dissolution rate. Additionally, as viscosity decreased, liquid-mass transfer occurred more easily and the mass transfer coefficient increased.

Author Contributions: Conceptualization, T.K., H.U. and Y.C.; Methodology, T.K., H.U.; Validation, T.K.; Investigation, T.K.; Writing – original draft, T.K.; Writing – review & editing, H.U. and Y.C.; Supervision, H.U. and Y.C.; Project administration, Y.C. All authors have read and agreed to the published version of the manuscript.

Funding: This research was funded by the Korea Evaluation Institute of Industrial Technology (KEIT) grant (Grant number 00262191, 00262711), and by the Korea Institute of Energy Technology Evaluation and Planning (KETEP) grant (Grant number 20212010100060).

Data Availability Statement: No data available.

Conflicts of Interest: The authors declare no conflict of interest.

References

1. Fan, Z.; Friedmann, S.J. Low-carbon production of iron and steel: Technology options, economic assessment, and policy. *Joule* **2021**, *5*, 829–862. [[CrossRef](#)]
2. Lee, B.; Sohn, I. Review of Innovative Energy Savings Technology for the Electric Arc Furnace. *JOM* **2014**, *66*, 1581–1594. [[CrossRef](#)]
3. Park, J.H.; Todoroki, H. Control of $\text{MgO}\cdot\text{Al}_2\text{O}_3$ spinel inclusions in stainless steels. *ISIJ Int.* **2010**, *50*, 1333–1346. [[CrossRef](#)]
4. Dimitrov, S.; Weyl, A.; Janke, D. Control of the aluminium-oxygen reaction in pure iron melts. *Steel Res.* **1995**, *66*, 3–7. [[CrossRef](#)]
5. Um, H.; Yeo, S.; Kang, Y.-B.; Chung, Y. The effect of Fe_xO content on dissolution behavior of an alumina inclusion in $\text{CaO}\text{-Al}_2\text{O}_3\text{-SiO}_2\text{-Fe}_x\text{O}$ slag by a single hot thermocouple technique. *Ceram. Int.* **2022**, *48*, 35301–35309. [[CrossRef](#)]

6. Jung, I.-H.; Deckerov, S.A.; Pelton, A.D. Computer applications of thermodynamic databases to inclusion engineering. *ISIJ Int.* **2004**, *44*, 527–536. [[CrossRef](#)]
7. Holappa, L.; Hämäläinen, M.; Liukkonen, M.; Lind, M. Thermodynamic examination of inclusion modification and precipitation from calcium treatment to solidified steel. *Ironmak. Steelmak.* **2003**, *30*, 111–115. [[CrossRef](#)]
8. Park, J.-H.; Jung, I.-H.; Hae-Geon, L.E.E. Dissolution behavior of Al_2O_3 and MgO inclusions in the $\text{CaO-Al}_2\text{O}_3\text{-SiO}_2$ slags: Formation of ring-like structure of MgAl_2O_4 and Ca_2SiO_4 around MgO inclusions. *ISIJ Int.* **2006**, *46*, 1626–1634. [[CrossRef](#)]
9. Sridhar, S.; Cramb, A.W. Kinetics of Al_2O_3 dissolution in $\text{CaO-MgO-SiO}_2\text{-Al}_2\text{O}_3$ slags: In situ observations and analysis. *Metall. Mater. Trans. B Process Metall. Mater. Process. Sci.* **2000**, *31*, 406–410. [[CrossRef](#)]
10. Shu, Q.; Zhang, X.; Wang, Y.; Li, J.; Chou, K. Effect of Na_2O on dissolution rate of alumina in $\text{CaO-Al}_2\text{O}_3\text{-MgO-SiO}_2$ slag. In Proceedings of the 6th International Congress on the Science and Technology of Steelmaking, ICS, Beijing, China, 12–14 May 2015; pp. 606–609.
11. Yi, K.W.; Tse, C.; Park, J.-H.; Valdez, M.; Cramb, A.W.; Sridhar, S. Determination of dissolution time of Al_2O_3 and MgO inclusions in synthetic $\text{Al}_2\text{O}_3\text{-CaO-MgO}$ slags. *Scand. J. Metall.* **2003**, *32*, 177–184. [[CrossRef](#)]
12. Ren, C.; Zhang, L.; Zhang, J.; Wu, S.; Zhu, P.; Ren, Y. In Situ Observation of the Dissolution of Al_2O_3 Particles in $\text{CaO-Al}_2\text{O}_3\text{-SiO}_2$ Slags. *Metall. Mater. Trans. B Process Metall. Mater. Process. Sci.* **2021**, *52*, 3288–3301. [[CrossRef](#)]
13. Holappa, L.; Kekkonen, M.; Louhenkilpi, S.; Hagemann, R.; Schröder, C.; Scheller, P. Active tundish slag. *Steel Res. Int.* **2013**, *84*, 638–648. [[CrossRef](#)]
14. Park, Y.-J.; Cho, Y.-M.; Cha, W.-Y.; Kang, Y.-B. Dissolution kinetics of alumina in molten $\text{CaO-Al}_2\text{O}_3\text{-Fe}_t\text{O-MgO-SiO}_2$ oxide representing the RH slag in steelmaking process. *J. Am. Ceram. Soc.* **2020**, *103*, 2210–2224. [[CrossRef](#)]
15. Yeo, S.; Um, H.; Chung, Y. The Effect of Alumina Activity on Dissolution Behavior of Alumina Particles in $\text{CaO-Al}_2\text{O}_3\text{-SiO}_2$ Slags. *Metall. Mater. Trans. B Process Metall. Mater. Process. Sci.* **2021**, *52*, 3938–3945. [[CrossRef](#)]
16. Zhang, S.; Rezaie, H.R.; Sarpoolaky, H.; Lee, W.E. Alumina dissolution into silicate slag. *J. Am. Ceram. Soc.* **2000**, *83*, 897–903. [[CrossRef](#)]
17. Valdez, M.; Prapakorn, K.; Cramb, A.W.; Seetharaman, S. A study of the dissolution of Al_2O_3 , MgO and MgAl_2O_4 particles in a $\text{CaO-Al}_2\text{O}_3\text{-SiO}_2$ slag. *Steel Res.* **2001**, *72*, 291–297. [[CrossRef](#)]
18. Monaghan, B.J.; Chen, L.; Sorbe, J. Comparative study of oxide inclusion dissolution in $\text{CaO-SiO}_2\text{-Al}_2\text{O}_3$ slag. *Ironmak. Steelmak.* **2005**, *32*, 258–264. [[CrossRef](#)]
19. Chen, G.; He, S.; Wang, Q. Dissolution behavior of Al_2O_3 into tundish slag for high-al steel. *J. Mater. Res. Technol.* **2020**, *9*, 11311–11318. [[CrossRef](#)]
20. Shi, G.-Y.; Zhang, T.-A.; Dou, Z.-H.; Niu, L.-P. Dissolution behavior of Al_2O_3 inclusions in $\text{CaO-Al}_2\text{O}_3$ based slag representing aluminothermic reduction slag. *Crystals* **2020**, *10*, 1061. [[CrossRef](#)]
21. Odenthal, H.-J.; Kemminger, A.; Krause, F.; Sankowski, L.; Uebber, N.; Vogl, N. Review on Modeling and Simulation of the Electric Arc Furnace (EAF). *Steel Res. Int.* **2018**, *89*, 1700098. [[CrossRef](#)]
22. Lee, S.; Chung, Y. The effect of C content in MgO-C on dissolution behavior in $\text{CaO-SiO}_2\text{-Al}_2\text{O}_3$ slag. *Ceram. Int.* **2022**, *48*, 26984–26991. [[CrossRef](#)]
23. Kim, Y.; Kashiwaya, Y.; Chung, Y. Effect of varying Al_2O_3 contents of $\text{CaO-Al}_2\text{O}_3\text{-SiO}_2$ slags on lumped MgO dissolution. *Ceram. Int.* **2020**, *46*, 6205–6211. [[CrossRef](#)]
24. Taira, S.; Nakashima, K.; Mori, K. Kinetic Behavior of Dissolution of Sintered Alumina Into $\text{CaO-SiO}_2\text{-Al}_2\text{O}_3$ Slags. *ISIJ Int.* **1993**, *33*, 116–123. [[CrossRef](#)]
25. Choi, J.-Y.; Lee, H.-G.; Kim, J.-S. Dissolution rate of Al_2O_3 into molten $\text{CaO-SiO}_2\text{-Al}_2\text{O}_3$ slags. *ISIJ Int.* **2002**, *42*, 852–860. [[CrossRef](#)]
26. Samaddar, B.N.; Kingery, W.D.; Cooper, A.R. Dissolution in Ceramic Systems: 11, Dissolution of Aluminum, Mullite, Anorthite, and Silica in a Calcium-Aluminum-Silicate Slag. *J. Am. Ceram. Soc.* **1964**, *47*, 249–254. [[CrossRef](#)]
27. Oishi, Y.; Cooper, A.R.; Kingery, W.D. Dissolution in Ceramic Systems: III, Boundary Layer Concentration Gradients. *J. Am. Ceram. Soc.* **1965**, *48*, 88–95. [[CrossRef](#)]
28. Bui, A.-H.; Ha, H.-M.; Kang, Y.-B.; Chung, I.-S.; Lee, H.-G. Dissolution behavior of alumina in mold fluxes for steel continuous casting. *Met. Mater. Int.* **2005**, *11*, 183–190. [[CrossRef](#)]
29. Yan, P.; Webler, B.A.; Pistorius, P.C.; Fruehan, R.J. Nature of MgO and Al_2O_3 Dissolution in Metallurgical Slags. *Metall. Mater. Trans. B Process Metall. Mater. Process. Sci.* **2015**, *46*, 2414–2418. [[CrossRef](#)]
30. Sharma, M.; Mu, W.; Dogan, N. In Situ Observation of Dissolution of Oxide Inclusions in Steelmaking Slags. *JOM* **2018**, *70*, 1220–1224. [[CrossRef](#)]
31. Cho, W.D.; Fan, P. Diffusional Dissolution of Alumina in Various Steelmaking Slags. *ISIJ Int.* **2004**, *44*, 229–234. [[CrossRef](#)]
32. Petrucci, R.H.; Harwood, W.S. *General Chemistry*, 6th ed.; Macmillan: New York, NY, USA, 1993; p. 535.
33. Liu, Y.Q.; Wang, L.J.; Chou, K.C. Dissolution behavior of Al_2O_3 in refining slags containing Ce_2O_3 . *ISIJ Int.* **2014**, *54*, 728–733. [[CrossRef](#)]

34. Park, J.S.; Park, J.H. Effect of Physicochemical Properties of Slag and Flux on the Removal Rate of Oxide Inclusion from Molten Steel. *Metall. Mater. Trans. B Process Metall. Mater. Process. Sci.* **2016**, *47*, 3225–3230. [[CrossRef](#)]
35. Valdez, M.; Shannon, G.S.; Sridhar, S. The ability of slags to absorb solid oxide inclusions. *ISIJ Int.* **2006**, *46*, 450–457. [[CrossRef](#)]

Disclaimer/Publisher’s Note: The statements, opinions and data contained in all publications are solely those of the individual author(s) and contributor(s) and not of MDPI and/or the editor(s). MDPI and/or the editor(s) disclaim responsibility for any injury to people or property resulting from any ideas, methods, instructions or products referred to in the content.